

# The effect of carbon and rare earth oxide co-doping on the structural and superconducting properties of $\text{MgB}_2$

N Ojha<sup>1</sup>, V K Malik<sup>2</sup>, Rashmi Singla<sup>1</sup>, C Bernhard<sup>2</sup> and G D Varma<sup>1,3</sup>

<sup>1</sup> Department of Physics, Indian Institute of Technology Roorkee, Roorkee-247667, India

<sup>2</sup> Department of Physics and Fribourg Centre for Nanomaterials-FriMat, University of Fribourg, Chemin du Musée, CH-1700 Fribourg, Switzerland

E-mail: [gdvarfph@iitr.ernet.in](mailto:gdvarfph@iitr.ernet.in)

## Abstract

Carbon (C) and rare earth oxide (REO) co-doped bulk polycrystalline  $\text{MgB}_2$  samples with nominal compositions  $\text{Mg}_{1-y}(\text{REO})_y(\text{B}_{0.95}\text{C}_{0.05})_2$  (where  $y = 0.00, 0.01, 0.03, 0.05$  and  $\text{REO} = \text{Eu}_2\text{O}_3$  or  $\text{Pr}_6\text{O}_{11}$ ) have been synthesized via a solid state reaction route. The XRD results reveal the presence of impurity phases  $\text{EuB}_6$  in  $\text{Eu}_2\text{O}_3$  and  $\text{PrB}_4$  and  $\text{PrB}_6$  in  $\text{Pr}_6\text{O}_{11}$  co-doped samples along with the main hexagonal phase of  $\text{MgB}_2$  and a small amount of  $\text{MgO}$ . The values of upper critical field ( $H_{c2}$ ) and irreversibility field ( $H_{\text{irr}}$ ), except  $H_{c2}$  of  $y = 0.05$  for  $\text{Eu}_2\text{O}_3$ , have been found to increase at all temperatures ( $< T_c$ ) with increasing doping concentration of REO. Improvements in the values of critical current density ( $J_c$ ) at 10 K for  $y = 0.01$  of  $\text{Eu}_2\text{O}_3$  and  $y = 0.01, 0.03$  of  $\text{Pr}_6\text{O}_{11}$  co-doped samples have been observed in high fields ( $> 6.5$  T) region. At 20 K enhancement in the high field ( $> 6$  T)  $J_c$  values for  $y = 0.01, 0.03$  of  $\text{Eu}_2\text{O}_3$  and  $y = 0.01$  of  $\text{Pr}_6\text{O}_{11}$  co-doped samples are also reported in the present work. The correlations between the structural characteristics and the observed superconducting properties of the co-doped samples are described and discussed in this paper.

## 1. Introduction

The  $\text{MgB}_2$  superconductor is expected to be a promising material for practical applications because of its high transition temperature ( $T_c$ ), simple composition, lack of a weak link problem and low cost [1, 2]. Much effort has been made since the discovery of superconductivity in  $\text{MgB}_2$  to enhance its superconducting properties, mainly the upper critical magnetic field ( $H_{c2}$ ), irreversibility field ( $H_{\text{irr}}$ ) and in-field critical current density ( $J_c(H)$ ), to the level required for technological applications [3]. Chemical doping has been found very effective in improving the superconducting properties of  $\text{MgB}_2$  [3–12]. Although many doping elements and compounds have been used as dopants, the substitution of C for B, using various sources of C such as SiC, C,

$\text{B}_4\text{C}$ , carbon nanotubes and carbohydrates [6, 13–27], has been found very effective in improving the superconducting properties of  $\text{MgB}_2$ . It is believed that the C substitution for boron enhances  $H_{c2}$  while the defects and grain boundaries are responsible for flux pinning [28]. C substitution for boron induces disorder in lattice sites, which leads to enhancement in  $H_{c2}$ . The excess carbon and impurity phases in the C doped samples can be embedded within the  $\text{MgB}_2$  grains as nano-inclusions, which lead to enhancement in flux pinning. In addition to C, recently it has been observed that doping of rare earth oxides in  $\text{MgB}_2$  significantly improve its superconducting properties [9, 30–36]. It has been seen that even though rare earth elements (RE) possess a magnetic moment they do not greatly suppress the superconductivity of  $\text{MgB}_2$  [9, 31–35]. For example Chen *et al* [9] have found a significant enhancement in  $J_c$  in a low or medium field for 0.5–5.0 wt%  $\text{Dy}_2\text{O}_3$  doped  $\text{MgB}_2$ . Cheng *et al*

<sup>3</sup> Author to whom any correspondence should be addressed.

[32] have found no change in crystal structure,  $T_c$  or  $H_{c2}$  but a significant enhancement in  $J_c$  and  $H_{irr}$  for 0.1-10%  $\text{Ho}_2\text{O}_3$  doped  $\text{MgB}_2$ . A similar study on  $\text{Pr}_6\text{O}_{11}$  doped  $\text{MgB}_2$  has shown improvement in  $J_c$  and  $H_{irr}$  for low level doping ( $\sim 1$  wt%) and a degradation in performance of  $\text{MgB}_2$  for higher doping levels [33]. Our investigations on  $\text{Pr}_6\text{O}_{11}$  and  $\text{Eu}_2\text{O}_3$  doped  $\text{MgB}_2$  samples also revealed improvement in  $H_{c2}$ ,  $H_{irr}$  and  $J_c(H)$  without much degradation in  $T_c$  [34–36]. Based on the results of various groups it has been found that the possible reasons for improvement in the superconducting properties of rare earth oxide doped  $\text{MgB}_2$  are an enhancement in the flux pinning due to magnetic impurity phases within the grains of  $\text{MgB}_2$ , and lattice distortions. In the case of C doped  $\text{MgB}_2$  the enhancement in  $H_{c2}$  takes place due to the lattice distortion on C substitution for B. Thus it appears that by simultaneous doping of C and rare earth oxide the superconducting properties of  $\text{MgB}_2$  may be further improved. Earlier Flükiger *et al* [29] have shown improvement in  $J_c(H)$  and  $B_{irr}$  of  $\text{B}_4\text{C}$  and  $\text{SiC}$  co-doped  $\text{MgB}_2$  samples. Therefore, in order to study the combined effect of both C substitution and rare earth oxide doping on the structural and superconducting properties of  $\text{MgB}_2$  we have synthesized the  $\text{Pr}_6\text{O}_{11}/\text{Eu}_2\text{O}_3$  and C co-doped  $\text{MgB}_2$  samples via solid state reaction route. The composition of C in  $\text{MgB}_2$  is generally expressed by the formula  $\text{Mg}(\text{B}_{1-x}\text{C}_x)_2$  and the best results have been found for  $x = 0.05$  [12, 37, 38]. Hence, in the present case, we have synthesized samples with nominal compositions  $\text{Mg}_{1-y}(\text{REO})_y(\text{B}_{0.95}\text{C}_{0.05})_2$  (where  $y = 0.00, 0.01, 0.03, 0.05$  and  $\text{REO} = \text{Eu}_2\text{O}_3$  or  $\text{Pr}_6\text{O}_{11}$ ) and studied the variation in the structural and superconducting properties ( $H_{c2}$ ,  $H_{irr}$  and  $J_c(H)$ ) with the composition of rare earth oxide in the samples.

## 2. Experimental details

The rare earth oxide and C co-doped  $\text{MgB}_2$  samples have been synthesized with nominal compositions  $\text{Mg}_{1-y}(\text{REO})_y(\text{B}_{0.95}\text{C}_{0.05})_2$  (where  $y = 0.00, 0.01, 0.03, 0.05$  and  $\text{REO} = \text{Eu}_2\text{O}_3$  or  $\text{Pr}_6\text{O}_{11}$ ) via a solid state reaction route. Appropriate amounts of Mg, B, graphite and  $\text{Eu}_2\text{O}_3$ , or  $\text{Pr}_6\text{O}_{11}$ , were mixed and ground in an agate mortar. The resulting powder was pelletized in the form of rectangular pellets. The pellets were sintered at  $\sim 850^\circ\text{C}$  in flowing Ar for  $\sim 3$  h and finally cooled down to room temperature by switching off the furnace. Henceforth, the undoped samples and co-doped samples with  $\text{Eu}_2\text{O}_3$  compositions  $y = 0.0, 0.01, 0.03$  and  $0.05$  will be represented as MB, MBC, MBCE1, MBCE3 and MBCE5, respectively. Similarly,  $\text{Pr}_6\text{O}_{11}$  co-doped samples with compositions  $y = 0.01, 0.03$  and  $0.05$  will be represented as MBCP1, MBCP3 and MBCP5, respectively. The samples were characterized by x-ray diffraction (XRD) for phase identification. The microstructural properties were studied by FESEM. The resistivity transitions in fields up to 8 T were measured by a Physical Properties Measurement Systems (PPMS-Quantum Design 6000).  $H_{c2}$  and  $H_{irr}$  were estimated from the resistive transition curves using the criteria 90% and 10% of the normal state resistivity, respectively [39]. The magnetization of samples was measured at 10 and 20 K using PPMS. The magnetic  $J_c$  values were calculated from

the width of the magnetization loop  $\Delta M$  using the formula  $J_c = 30\Delta M/d$ , where ‘ $d$ ’ is the average grain size [40].

## 3. Results and discussion

Figure 1 shows the XRD patterns of the co-doped and undoped  $\text{MgB}_2$  samples synthesized in the present work. The XRD patterns of samples MB and MBC reveal the presence of a dominant hexagonal crystal structure of  $\text{MgB}_2$  with only a small amount of impurity phase  $\text{MgO}$ . On the other hand, XRD patterns of  $\text{Eu}_2\text{O}_3$  co-doped  $\text{MgB}_2$  samples show, besides  $\text{MgO}$ , the presence of an impurity phase  $\text{EuB}_6$  and the intensities of the peaks of this phase increase with increasing doping level of  $\text{Eu}_2\text{O}_3$  in the samples. In addition to the peaks of impurity phases  $\text{EuB}_6$  and  $\text{MgO}$ , the peak of a  $\text{EuC}_2$  impurity phase is observed at  $2\theta \sim 26^\circ$  in the XRD patterns of  $\text{Eu}_2\text{O}_3$  co-doped samples (see figure 1(a)). The impurity phase  $\text{EuC}_2$  forms due to reaction of Eu and C present in the reaction mixture. The intensity of this peak, however, decreases with increasing doping level of  $\text{Eu}_2\text{O}_3$ . As we have synthesized the samples with fixed C concentration, the ratio of C and Eu in the sample decreases with increasing  $\text{Eu}_2\text{O}_3$  content in the samples. Possibly due to this there is decrease in the intensity of the  $\text{EuC}_2$  peak with increasing  $\text{Eu}_2\text{O}_3$  content in the sample. In  $\text{Pr}_6\text{O}_{11}$  co-doped  $\text{MgB}_2$  samples, besides  $\text{MgO}$ , impurity phases  $\text{PrB}_6$  and  $\text{PrB}_4$  have been detected through XRD results. Like the  $\text{Eu}_2\text{O}_3$  co-doped samples in this case the intensities of these impurity phases also increase with increasing doping level of  $\text{Pr}_6\text{O}_{11}$ . Moreover, comparison of the XRD patterns of  $\text{Eu}_2\text{O}_3$  and  $\text{Pr}_6\text{O}_{11}$  co-doped samples reveals that the  $\text{MgO}$  peaks are more intense in the XRD patterns of  $\text{Pr}_6\text{O}_{11}$  co-doped samples as compared to the corresponding  $\text{Eu}_2\text{O}_3$  co-doped ones. This is possibly due to more oxygen atoms in the dopant  $\text{Pr}_6\text{O}_{11}$  as compared to the dopant  $\text{Eu}_2\text{O}_3$ . From the XRD patterns it can be seen that the intensity of the  $\text{MgO}$  peak increases with increasing doping concentration of  $\text{Pr}_6\text{O}_{11}$  in the sample. This result shows that the  $\text{MgO}$  content in the sample increases with increasing doping concentration of  $\text{Pr}_6\text{O}_{11}$  in the sample. The peaks of all the impurity phases have been marked in figure 1. The lattice parameters calculated from the XRD results are given in table 1(a) and (b) for  $\text{Eu}_2\text{O}_3$  and  $\text{Pr}_6\text{O}_{11}$  co-doped samples, respectively. Here it can be seen that the lattice parameters  $a$  and  $c$  of sample MBC have lower values as compared to sample MB, this confirms the substitution of C for the B of  $\text{MgB}_2$ . This result is consistent with the previous results of C doped samples [13–15]. Furthermore, the lattice parameters  $a$  and  $c$  decrease with increasing doping concentration of REO in the samples. As the ionic radii of  $\text{Eu}^{3+}$  and  $\text{Pr}^{3+}$  are larger than that of  $\text{Mg}^{2+}$ , this decrease in the lattice parameters due to the substitution of a rare earth element for the Mg of  $\text{MgB}_2$  is ruled out. It can be seen that the FWHM values of the (101) peak increases from 0.294 to 0.481 for  $\text{Eu}_2\text{O}_3$  doped samples and from 0.294 to 0.581 for  $\text{Pr}_6\text{O}_{11}$  doped samples when values of  $y$  increase from 0.01 to 0.05 (see table 1(a) and (b)). This indicates that the crystallinity of the samples decreases with increasing doping level [18, 41]. We have estimated the strain values and crystallite sizes of the samples from the Williamson–Hall plots [42]. It has been

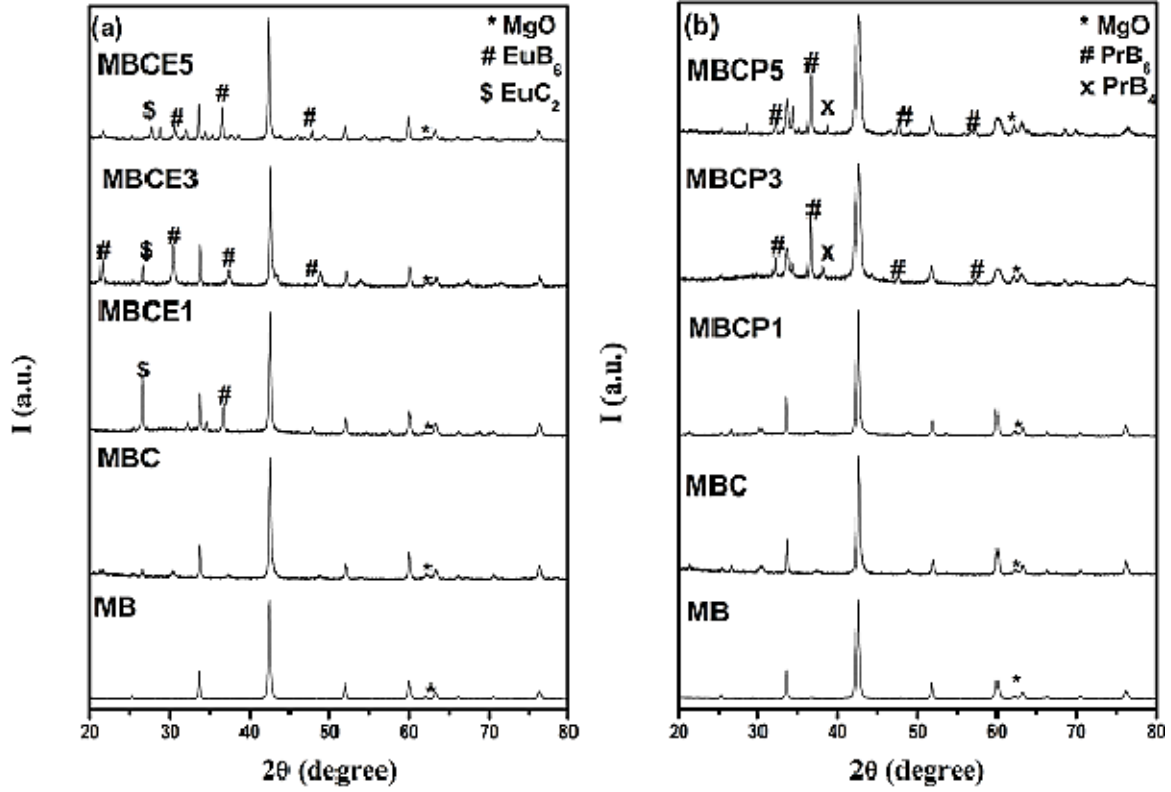


Figure 1. XRD patterns of undoped and co-doped  $\text{MgB}_2$  samples.

**Table 1.** (a) Various parameters of undoped and  $\text{Eu}_2\text{O}_3$  co-doped  $\text{MgB}_2$  samples. (b) Various parameters of undoped and  $\text{Pr}_6\text{O}_{11}$  co-doped  $\text{MgB}_2$  samples.

Samples	Lattice parameter (Å)		$T_C$ (K)	FWHM (101)	RRR	Crystallite size ( $\mu\text{m}$ )	Vol% of MgO	Strain	$A_F$
	$a$	$c$							
(a)									
MB	3.0861	3.5222	38.30	0.294	3.35	0.621	1.6	0.025	0.238
MBC	3.0581	3.5180	37.98	0.304	3.12	0.525	2.6	0.026	0.231
MBCE1	3.0551	3.5114	37.81	0.344	3.05	0.483	1.7	0.027	0.224
MBCE3	3.0455	3.5102	37.49	0.377	2.86	0.445	2.0	0.031	0.192
MBCE5	3.0432	3.4950	35.89	0.481	2.70	0.427	3.1	0.035	0.165
(b)									
MB	3.0861	3.5222	38.30	0.294	3.35	0.621	1.6	0.025	0.238
MBC	3.0581	3.5180	37.98	0.304	3.12	0.525	2.6	0.026	0.231
MBCP1	3.0523	3.5163	35.51	0.362	2.95	0.503	2.9	0.032	0.271
MBCP3	3.0478	3.5129	35.17	0.571	2.74	0.472	3.2	0.038	0.248
MBCP5	3.0472	3.5003	33.33	0.582	2.51	0.468	3.6	0.044	0.185

found that the values of microstrain increase and the crystallite sizes decrease with increasing doping concentration of REO (see table 1(a) and (b)). The increase in strain value with doping is suggestive of a corresponding increase in lattice defect in the co-doped samples, and possibly due to this there is a decrease in the lattice parameters and a reduction in the crystallite size with increasing doping level. The decreased crystallite size helps to enhance the flux pinning, since grain boundaries act as strong pinning centers [18, 43].

The zero resistance ( $R = 0$ ) transition temperatures ( $T_c$ ) of all the samples have been determined from the R-T measurements (figure not shown here) in zero field, and their values are given in table 1(a) and (b), respectively, for  $\text{Eu}_2\text{O}_3$

and  $\text{Pr}_6\text{O}_{11}$  co-doped samples. It can be seen that, as usual,  $T_c$  decreases on C doping and it further decreases with increasing doping level of REO in the samples. The decrease in  $T_c$  on C doping is consistent with the earlier results of C doped  $\text{MgB}_2$  samples [24]. However, in the present case, the reduction in the  $T_c$  of the C doped sample is less. In the present case, possibly increased disorder is responsible for the decrease in  $T_c$  values with increasing REO concentration in the co-doped samples [18, 44–46]. Comparison of the  $T_c$  values of  $\text{Eu}_2\text{O}_3$  and  $\text{Pr}_6\text{O}_{11}$  co-doped samples show higher values of  $T_c$  for  $\text{Eu}_2\text{O}_3$  co-doped samples as compared to the corresponding  $\text{Pr}_6\text{O}_{11}$  co-doped ones. This result is also consistent with the microstrain values of REO doped samples, i.e. the samples

with lower values of microstrain, i.e. less disorder, have higher values of  $T_c$  (see table 1(a) and (b)). From the XRD results we have also seen higher MgO content in the  $\text{Pr}_6\text{O}_{11}$  co-doped samples as compared to the corresponding  $\text{Eu}_2\text{O}_3$  co-doped ones. This may also be responsible for the lower value of  $T_c$  for  $\text{Pr}_6\text{O}_{11}$  co-doped samples as compared to the corresponding  $\text{Eu}_2\text{O}_3$  co-doped ones. From the R-T measurement it has been found that the residual resistivity ratio ( $\text{RRR} = R_{300\text{ K}}/R_{40\text{ K}}$ ) values continuously decreases with increasing doping level. This is due to an increase in the amount of impurity phases with increasing doping concentration in the samples. From the table 1(a) and (b) we can see that the RRR values of  $\text{Pr}_6\text{O}_{11}$  co-doped samples have lower values as compared to the corresponding  $\text{Eu}_2\text{O}_3$  co-doped ones. This result again indicates a higher concentration of impurity phases in  $\text{Pr}_6\text{O}_{11}$  co-doped samples, as suggested by the XRD results. The impurity phases can enhance the electron scattering, and hence a decrease in the RRR value [9]. The effective cross-sectional area, used to estimate the impurity scattering, has been calculated by the equation  $A_F = \Delta\rho_{\text{ideal}}/(\rho_{300\text{ K}} - \rho_{40\text{ K}})$ , proposed by Rowell [47].  $\Delta\rho_{\text{ideal}}$  is the ideal change in resistivity from 300 K to 40 K for a fully connected sample and its value is taken to be  $7.3\ \mu\Omega\text{ cm}$  [48]. The calculated values of  $A_F$  are given in table 1(a) and (b), respectively, for  $\text{Eu}_2\text{O}_3$  and  $\text{Pr}_6\text{O}_{11}$  co-doped samples. It can be seen that  $A_F$  values of the co-doped samples are smaller than that of the undoped one. This indicates poor connection and high intragrain scattering in the co-doped samples [49]. The poor connectivity due to the presence of impurity phases, such as MgO,  $\text{PrB}_6/\text{EuB}_6$ ,  $\text{PrB}_4$  and the extra C at the grain boundaries, and high intragrain scattering are responsible for the higher resistivity of the co-doped samples as compared to the undoped one.

The FESEM micrographs of the  $\text{Eu}_2\text{O}_3$  and  $\text{Pr}_6\text{O}_{11}$  co-doped samples are shown in figures 2 and 3, respectively. For comparison the FESEM micrographs of samples MB and MBC are also given in both figures. From the FESEM micrograph it is clear that the MB sample has a homogeneous microstructure as compared to the co-doped samples. On the other hand, FESEM micrographs of the co-doped samples reveal the presence of clusters of several smaller grains. This is the typical microstructural feature of the doped  $\text{MgB}_2$  samples reported earlier [50, 51]. Possibly due to precipitation of the impurity phases at the grain boundaries of  $\text{MgB}_2$ , some of the grains appear to be well connected together in the co-doped samples. Further, the impurity phases at the grain boundaries inhibit the grain growth, leading to smaller crystallite sizes of the co-doped samples. This result is in conformity with the XRD result.

$H_{c2}$  versus  $T/T_c$  and  $H_{\text{irr}}$  versus  $T/T_c$  plots of all the samples synthesized in the present work are shown in figures 4 and 5, respectively. From the plots we see an increase in the  $H_{c2}$  and  $H_{\text{irr}}$  values of sample MBC with respect to sample MB. This result is consistent with the earlier results of C doped samples [52–54]. Moreover, the values of  $H_{c2}$  and  $H_{\text{irr}}$  of co-doped samples as compared to samples MB and MBC further increase with increasing doping concentration of REO in the sample. Whereas the value of  $H_{c2}$  continuously increases with the doping concentration of  $\text{Pr}_6\text{O}_{11}$ , it increases

only up to  $y = 0.03$  for  $\text{Eu}_2\text{O}_3$  co-doped samples and after this it starts decreasing (see figure 4(a)). The values of  $H_{c2}$  of sample MBE5 are, however, higher than those of samples MB and MBC at all temperatures ( $<T_c$ ). On the other hand the values of  $H_{\text{irr}}$  continuously increase with increasing concentration of REO for both  $\text{Eu}_2\text{O}_3$  and  $\text{Pr}_6\text{O}_{11}$  co-doped samples. Furthermore, the comparison of the temperature dependence  $H_{c2}$  and  $H_{\text{irr}}$  of  $\text{Eu}_2\text{O}_3$  and  $\text{Pr}_6\text{O}_{11}$  co-doped samples show higher values of  $H_{c2}$  and  $H_{\text{irr}}$  at all temperatures for the latter dopant. In the present case enhancements of  $H_{c2}$  and  $H_{\text{irr}}$  values of co-doped samples are mainly due to the increased value of lattice strain. We also find a correlation between the FWHM of the (101) diffraction peak and the  $H_{\text{irr}}$  value as reported by Yamamoto *et al* [55]. This increased  $H_{\text{irr}}$  value of the co-doped samples is attributed to increased lattice distortions and impurity phases. The higher values of  $H_{\text{irr}}$  and  $H_{c2}$  of  $\text{Pr}_6\text{O}_{11}$  co-doped samples as compared to corresponding  $\text{Eu}_2\text{O}_3$  co-doped samples are possibly due to more lattice distortion and MgO content in the  $\text{Pr}_6\text{O}_{11}$  co-doped samples, which is evident from the microstrain value and MgO content of the samples given in table 1(a) and (b).

The field dependence of the  $J_c$  values of all the samples calculated from the M-H loops, measured at 10 and 20 K, using Bean's critical state model are shown in figure 6. The average crystallite sizes (estimated from the FESEM micrographs) used for the calculation of  $J_c$  values are given in table 1. It is seen that the self-field  $J_c$  of the doped samples have lower values as compared to that of the undoped samples. The most likely reason for this is increased lattice distortion and impurity phases such as MgO,  $\text{PrB}_6/\text{EuB}_6$  and unreacted C in the doped samples. In fields  $>2.5\text{ T}$  we see an improvement in the  $J_c(H)$  of sample MBC with respect to MB. This result is similar to earlier results for C doped samples [28, 41, 56]. In the case of  $\text{Eu}_2\text{O}_3$  co-doped samples at 10 K we see deterioration in the  $J_c(H)$  values as compared to sample MBC up to a field  $\sim 7\text{ T}$ , and in fields  $>7\text{ T}$  there is a slight improvement in the  $J_c(H)$  of samples MBCE1 and MBCE3 with respect to sample MBC. As compared to the undoped sample, however, there is an improvement in  $J_c(H)$  in fields  $>6.2\text{ T}$  for all compositions of  $\text{Eu}_2\text{O}_3$  with much improvement observed for sample MBCE1 (see figure 6(a)). At 20 K we find improvement in the  $J_c(H)$  of samples MBC, MBCE1, MBCE3 and a deterioration for sample MBCE5 as compared to MB in fields  $>2.5\text{ T}$ . Moreover, unlike at 10 K, here we see an improvement in the  $J_c$  of samples MBCE1 and MBCE3 as compared to MBC in fields  $>2.5\text{ T}$ . In the case of  $\text{Pr}_6\text{O}_{11}$  co-doped samples at 10 K and in the field range 2.5–6.5 T, the  $J_c(H)$  of the samples MBC, MBCP1 and MBCP3 have nearly the same values, but the values are higher as compared to sample MB. The  $J_c(H)$  value of sample MBCP5 has a lower value as compared to sample MB in the field range  $\sim 0\text{--}6\text{ T}$ , but there is an improvement in the  $J_c(H)$  value of this sample in the field  $>6\text{ T}$  with respect to the undoped sample (see figure 6(b)). In fields  $>6.5\text{ T}$  we see an improvement in the  $J_c(H)$  values of samples MBCP1, MBCP3 and MBCP5 as compared to those of samples MB and MBC. At 20 K and fields  $>4.5\text{ T}$ , we see an improvement in the  $J_c(H)$  values of all co-doped samples, but in the field range 4.6–6.0 T the



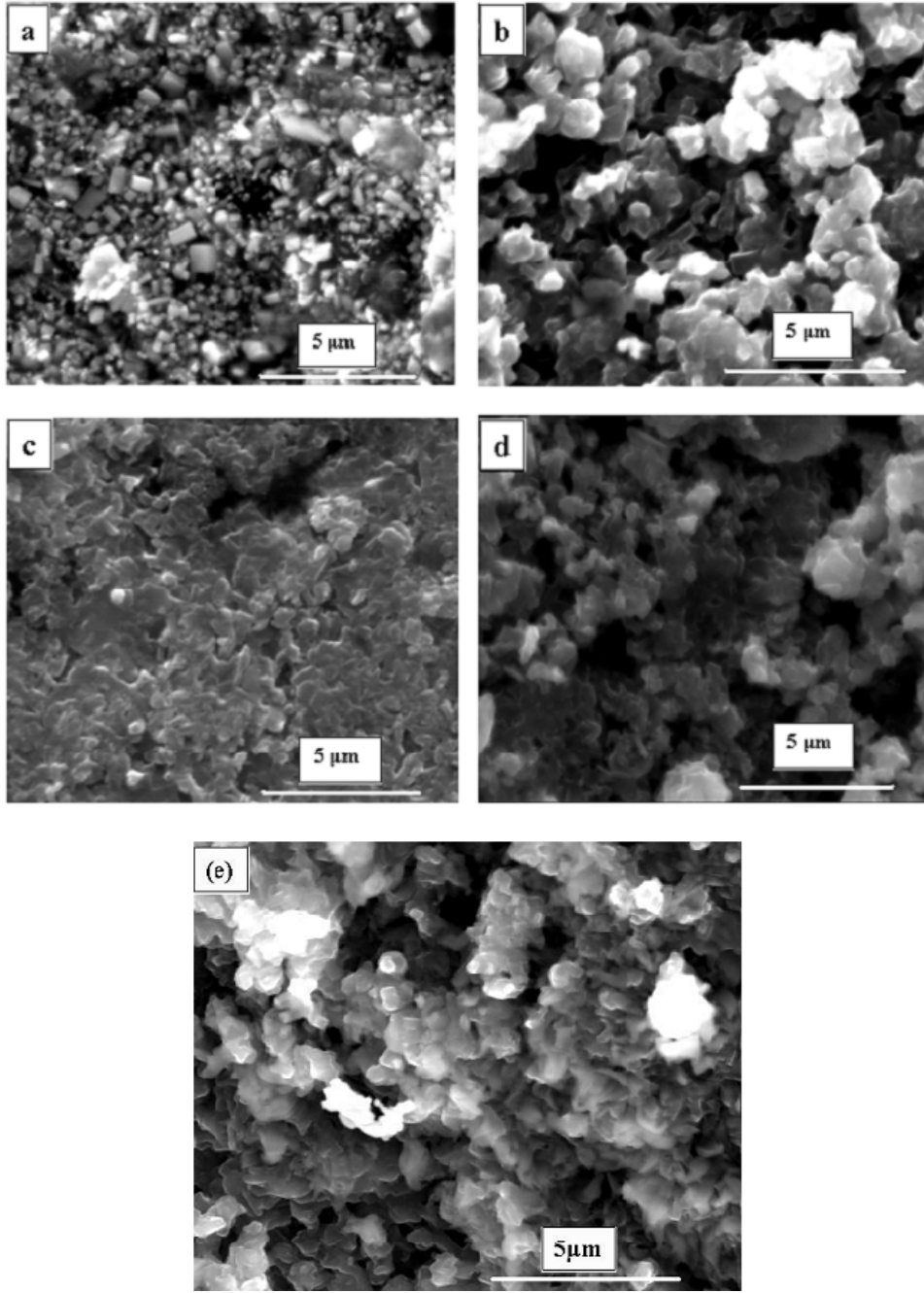


**Figure 2.** FESEM micrographs of samples MB (a), MBC (b), MBCE1 (c), MBCE3 (d) and MBCE5 (e).

$J_c(H)$  of co-doped samples have lower values as compared to sample MBC. There is, however, a small improvement in the  $J_c(H)$  of sample MBCP1 over sample MBC in fields  $>6.0$  T (see figure 6(d)). For comparison, the values of  $J_c(H = 0$  T),  $J_c(H = 5$  T) at 10 K and  $J_c(H = 0$  T),  $J_c(H = 4$  T) at 20 K of all samples are given in table 2. Thus, based on the present study of the field dependence of  $J_c$ , we find that in the case of  $\text{Eu}_2\text{O}_3$  co-doped samples there is a small improvement in high field ( $>6.5$  T)  $J_c(H)$  at 10 K only for sample MBCE1, but at 20 K we see slightly more improvement in a high field ( $>6$  T)  $J_c(H)$  for samples MBCE1 and MBCE3 as compared to the  $J_c(H)$  value of sample MBC at respective temperatures. On the other hand, in the case of  $\text{Pr}_6\text{O}_{11}$  co-doped samples, we

see slightly greater increase in a high field ( $>6.5$  T)  $J_c(H)$  at 10 K for samples MBCP1 and MBCP3 as compared to sample MBC, but at 20 K we see only a small improvement in high field ( $>6$  T)  $J_c(H)$  for sample MBCE1 over sample MBC.

In order to study the nature of pinning mechanisms we have calculated the volume pinning force,  $F_p = J_c \times H(T)$ , of undoped and doped samples at 20 K. The normalized volume pinning force  $f_p(h) = F_p/F_{p,\text{max}}$  (where  $F_{p,\text{max}}$  is the maximum pinning force) is plotted against the reduced magnetic field  $h = H/H_{\text{irr}}$  in figure 7 at 20 K. Here the  $H_{\text{irr}}$  value has been taken as the field at which  $J_c$  becomes  $100 \text{ A cm}^{-2}$ . It has been observed that if pinning arises due to a grain boundary,  $f_p$  follows a  $h^{0.5}(1 - h)^2$  dependence

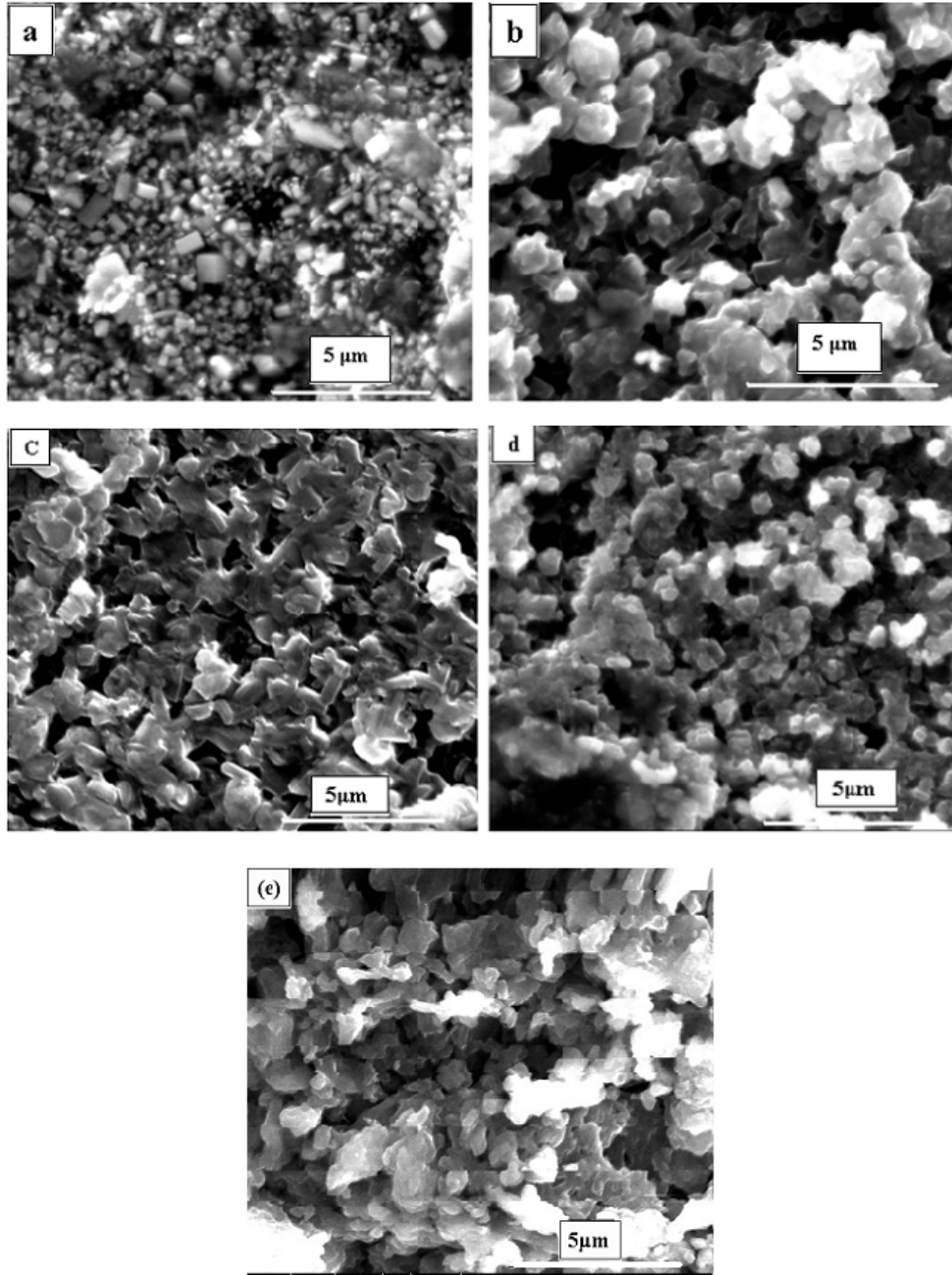


**Figure 3.** FESEM micrographs of samples MB (a), MBC (b), MBCP1 (c), MBCP3 (d) and MBCP5 (e).

**Table 2.** Critical current densities of undoped and co-doped  $\text{MgB}_2$  samples.

Samples	$J_C$ ( $\text{A cm}^{-2}$ )							
	$\text{Mg}_{1-y}(\text{Eu}_2\text{O}_3)_y(\text{B}_{0.95}\text{C}_{0.05})_2$				$\text{Mg}_{1-y}(\text{Pr}_6\text{O}_{11})_y(\text{B}_{0.95}\text{C}_{0.05})_2$			
	10 K		20 K		10 K		20 K	
	0 T	5 T	0 T	4 T	0 T	5 T	0 T	4 T
MB	$7.56 \times 10^5$	$4.83 \times 10^2$	$4.24 \times 10^5$	$1.82 \times 10^2$	$7.56 \times 10^5$	$4.83 \times 10^2$	$4.24 \times 10^5$	$1.82 \times 10^2$
$y = 0.00$	$2.76 \times 10^5$	$1.31 \times 10^3$	$1.74 \times 10^5$	$4.84 \times 10^2$	$2.76 \times 10^5$	$1.31 \times 10^3$	$1.74 \times 10^5$	$4.84 \times 10^2$
$y = 0.01$	$9.88 \times 10^4$	$1.67 \times 10^2$	$9.44 \times 10^4$	$1.03 \times 10^3$	$1.67 \times 10^5$	$2.18 \times 10^3$	$8.50 \times 10^4$	$2.83 \times 10^2$
$y = 0.03$	$5.84 \times 10^4$	$3.31 \times 10^2$	$6.11 \times 10^4$	$1.57 \times 10^3$	$1.29 \times 10^5$	$1.68 \times 10^3$	$3.47 \times 10^4$	$1.27 \times 10^2$
$y = 0.05$	$2.71 \times 10^4$	$3.88 \times 10^2$	$1.92 \times 10^4$	19.67	$3.91 \times 10^4$	$2.44 \times 10^2$	$1.45 \times 10^4$	88.31

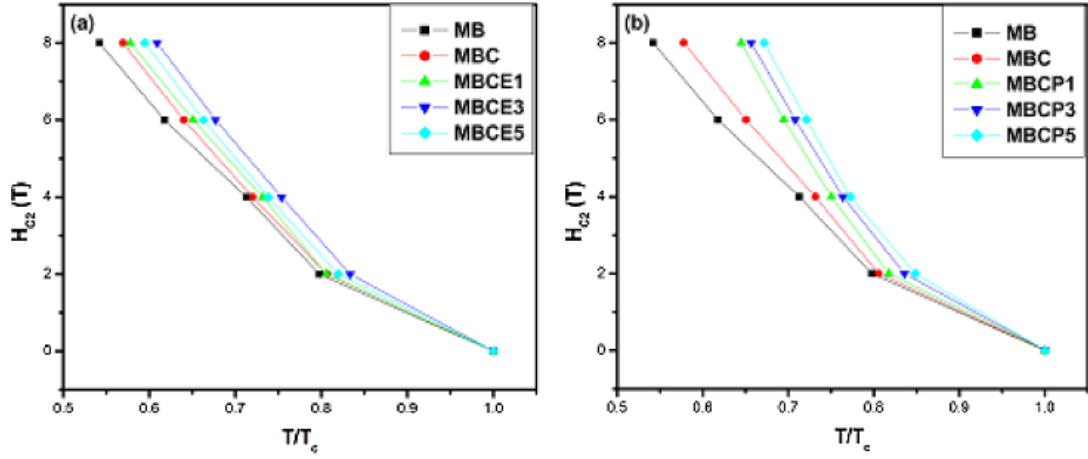


Figure 4.  $H_{c2}(T)$  versus  $T/T_c$  plots of undoped and co-doped  $\text{MgB}_2$  samples.

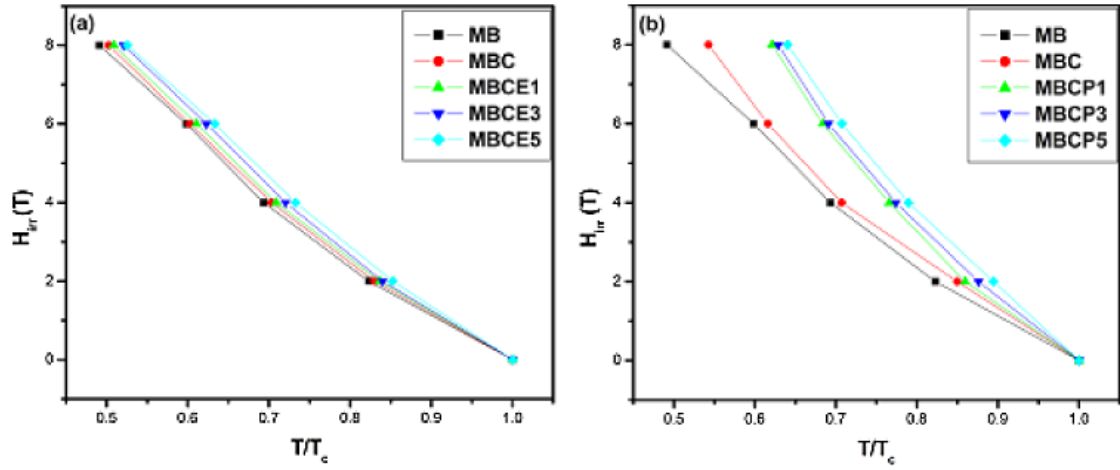


Figure 5.  $H_{irr}(T)$  versus  $T/T_c$  curves of undoped and co-doped  $\text{MgB}_2$  samples.

with a maximum value of  $f_p$  at  $h = 0.2$  [57, 58], and the  $f_p$  versus  $h$  curves overlap if a single pinning mechanism is involved. In our case the  $f_p$  versus  $h$  curves do not overlap and the maximum values of  $f_p$  occur for  $h_{max}$  varying in the range 0.13–0.20 (see figure 7); this suggests that there is more than one pinning mechanism involved in the samples. Further, the value of  $h_{max}$  increases with an increasing doping level of rare earth oxide in the samples. It can be seen from figure 7 that the values of  $f_p$  for  $h$  varying in the range 0.4–0.7 have higher values for co-doped samples as compared to those of MB and MBC. This may be explained in terms of two grain boundary pinning factors: grain size and the dirtiness of the superconducting matrix. It has been pointed out that electron scattering pinning at the grain boundary (known as  $\delta k$  pinning) is strongly dependent upon the purity of the sample [59]. From the XRD results we have seen that crystallinity decreases, and lattice distortion increases, with increasing doping concentration in the samples, which results in enhanced grain boundary flux pinning. Further, nanosized impurity phases such as  $\text{MgO}$ , unreacted C and other impurity phases ( $\text{EuB}_6/\text{PrB}_6$ ) present in the doped samples act as point pinning centers, leading to a slight improvement in their  $J_c(H)$  values.

#### 4. Conclusions

In summary, we have investigated the effect of REO and C co-doping on the superconducting properties of  $\text{MgB}_2$  produced by the solid state reaction method. The decrease in  $T_c$  value with increasing doping level is due to enhanced lattice distortion in the doped samples. Improvements in the  $H_{c2}$  and  $H_{irr}$  of co-doped samples have been observed as compared to samples MB and MBC. In the case of  $\text{Eu}_2\text{O}_3$  co-doped samples at 10 K a very small improvement in a high field ( $> 6.5 \text{ T}$ )  $J_c(H)$  of sample MBCE1, and at 20 K a moderate improvement in a high field ( $> 6 \text{ T}$ )  $J_c(H)$  of samples MBCE1 and MBCE3 as compared to the  $J_c(H)$  value of sample MBC at respective temperatures have been observed. In the case of  $\text{Pr}_6\text{O}_{11}$  co-doped samples, however, a slightly greater increase in a high field ( $> 6.5 \text{ T}$ )  $J_c(H)$  at 10 K of samples MBCP1 and MBCP3, and at 20 K only a marginal improvement in a high field ( $> 6 \text{ T}$ )  $J_c(H)$  of sample MBCP1 as compared to the  $J_c(H)$  value of sample MBC at respective temperatures have been observed. The enhancement of the  $H_{c2}$  and  $H_{irr}$  of co-doped samples is due to the introduction of impurity scattering centers in the  $\text{MgB}_2$  lattice. The improvement in the high field

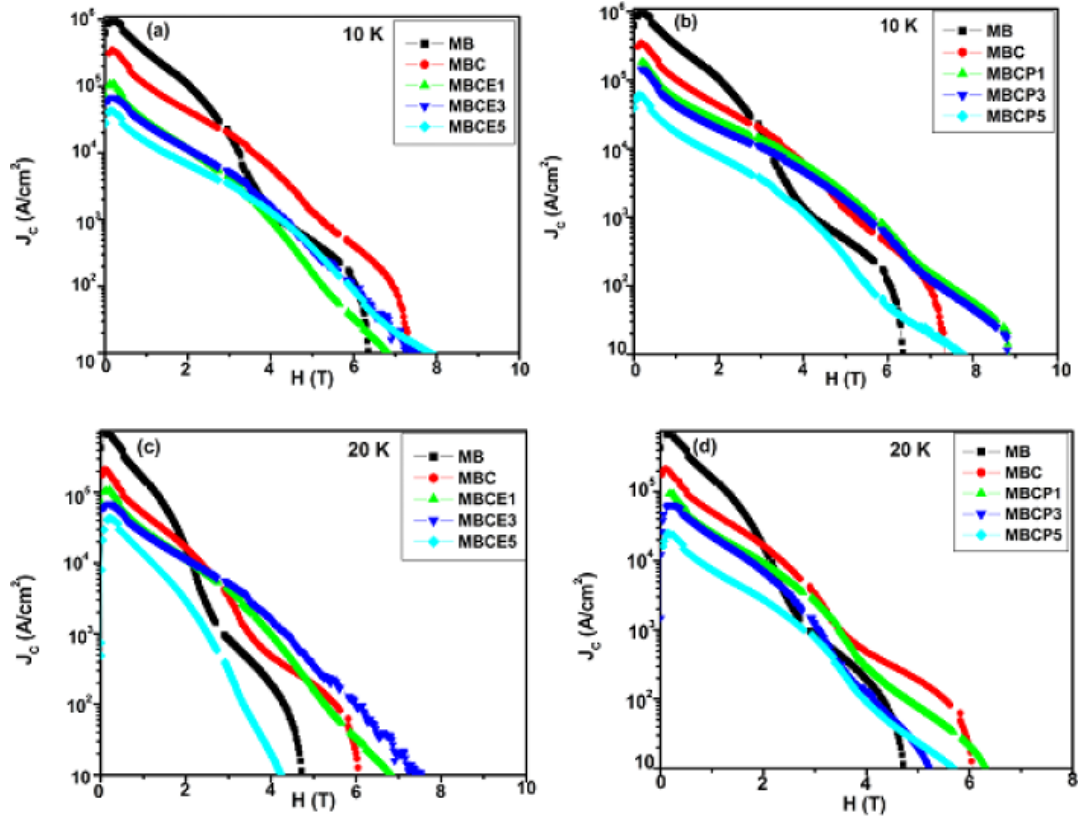


Figure 6.  $J_c(H)$  versus  $H(T)$  plots of undoped and co-doped  $\text{MgB}_2$  samples measured at 10 and 20 K.

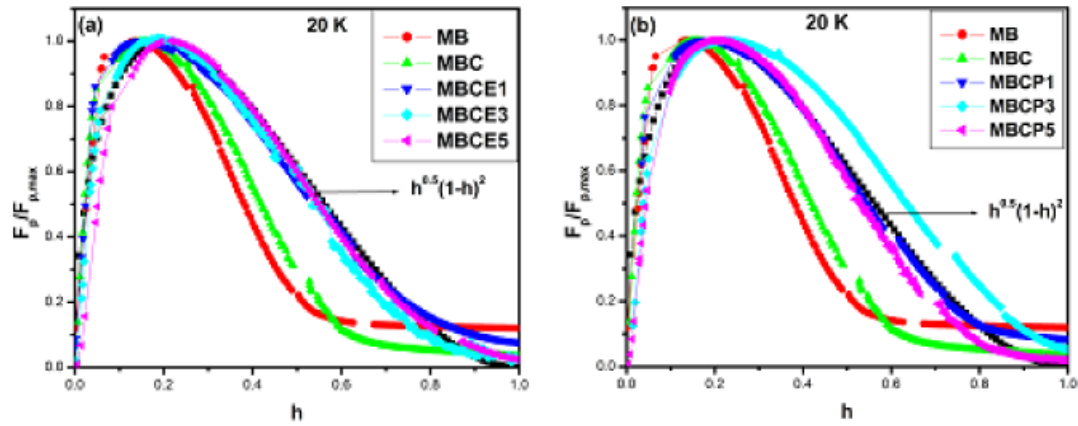


Figure 7.  $F_p/F_{p,\max}$  versus reduced field ( $h$ ) plots at 20 K of undoped and co-doped  $\text{MgB}_2$  samples.

$J_c(H)$  of some co-doped samples is due to the presence of impurity phases and lattice distortions.

### Acknowledgments

This work was financially supported by DST (Govt. of India) and C.S.I.R. (Govt. of India). We wish to thank Dr R Rawat (UGC-DAE CSR, Indore Centre) for carrying out R-T measurements in a magnetic field.

### References

- [1] Larbalestier D, Gurevich A, Feldmann D M and Polyanskii A 2001 *Nature* **414** 368
- [2] Buzea C and Yamashita T 2001 *Supercond. Sci. Technol.* **14** R115
- [3] Naito M and Ueda K 2004 *Supercond. Sci. Technol.* **17** R1
- [4] Serquis A *et al* 2002 *J. Appl. Phys.* **92** 351
- [5] Liao X Z, Serquis A, Zhu Y T, Huang J Y, Civale L, Peterson D E, Xu H F and Mueller F M 2003 *J. Appl. Phys.* **93** 6208
- [6] Dou S X, Soltanian S, Horvat J, Wang X L, Munroe P, Zhou S H, Ionescu M, Liu H K and Tomsic M 2002 *Appl. Phys. Lett.* **81** 3419
- [7] Zhou S H, Pan A V, Qin M J, Liu H K and Dou S X 2003 *Physica C* **387** 321
- [8] Berenov A, Serquis A, Liao X Z, Zhu Y T, Peterson D E, Bugoslavsky Y, Yates K A, Blamire M G, Cohen L F and MacManus-Driscoll J L 2004 *Supercond. Sci. Technol.* **17** 1093



- [9] Chen S K, Wei M and MacManus-Driscoll J L 2006 *Appl. Phys. Lett.* **88** 192512
- [10] Dou S X, Yeoh W K, Horvat J and Ionescu M 2003 *Appl. Phys. Lett.* **83** 4996
- [11] Yeoh W K, Horvat J, Dou S X and Munroe P 2005 *IEEE Trans. Appl. Supercond.* **15** 3284
- [12] Yeoh W K, Kim J H, Horvat J, Dou S X and Munroe P 2006 *Supercond. Sci. Technol.* **19** L5
- [13] Kumakura H, Kitaguchi H, Matsumoto A and Hatakeyama H 2005 *IEEE Trans. Appl. Supercond.* **15** 3184
- [14] Soltanian S, Wang X L, Horvat J, Dou S X, Sumption M D, Bhatia M, Collings E, Munroe P and Tomsic M 2005 *Supercond. Sci. Technol.* **18** 658
- [15] Yamamoto A, Shimoyama J, Ueda S, Katsura Y, Horii S and Kishio K 2005 *IEEE Trans. Appl. Supercond.* **15** 3292
- [16] Yan S C, Yan G, Lu Y F and Zhou L 2007 *Supercond. Sci. Technol.* **20** 549
- [17] Ma Y W, Zhang X P, Nishijima J, Watanabe K, Awaji S and Bai X D 2006 *Appl. Phys. Lett.* **88** 072502
- [18] Wilke R H T, Bud'ko S L, Canfield P C, Finnemore D K, Suplinskas R J and Hannahs S T 2004 *Phys. Rev. Lett.* **92** 217003
- [19] Yeoh W K, Kim J H, Horvat J, Xu X and Dou S X 2007 *Physica C* **460** 568
- [20] Yan S C, Yan G, Zhou L, Jia Y, Wen H H and Lu Y F 2007 *Supercond. Sci. Technol.* **20** 377
- [21] Mickelson W, Cumings J, Han W Q and Zettl A 2002 *Phys. Rev. B* **65** 052505
- [22] Yamamoto A, Shimoyama J, Ueda S, Iwayama I, Horii S and Kishio K 2005 *Supercond. Sci. Technol.* **18** 1323
- [23] Kim J H, Zhou S, Hossain M S A, Pan A V and Dou S X 2006 *Appl. Phys. Lett.* **89** 142505
- [24] Jun B H and Kim C J 2007 *Supercond. Sci. Technol.* **20** 980
- [25] Kim J H, Xu X, Hossain M S A, Shi D Q, Zhao Y, Wang X L, Dou S X, Choi S and Kiyoshi T 2008 *Appl. Phys. Lett.* **92** 042506
- [26] Shcherbakova O V, Pan A V, Wang J L, Shcherbakov A V, Dou S X, Wexler D, Babi'c E, Jerčinović M and Husnjak O 2008 *Supercond. Sci. Technol.* **21** 015005
- [27] Vajpayee A, Awana V P S, Bhalla A N, Bhoje P A, Nigam A K and Kishan H 2009 *Supercond. Sci. Technol.* **22** 015016
- [28] Zeng R, Lu L and Dou S X 2008 *Supercond. Sci. Technol.* **21** 085003
- [29] Flükiger R, Lezza P, Cesaretti M, Senatore C and Gladyshevskii R 2007 *IEEE Trans. Appl. Supercond.* **17** 2846
- [30] Vinod K, Neson V, Syamaprasad U, Shipra and Sundaresan A 2008 *Supercond. Sci. Technol.* **21** 025003
- [31] Wang J, Bugoslavsky Y, Berenov A, Cowey L, Caplin A D, Cohen L F, Driscoll J L M M, Cooley L D, Song X and Larbalestier D C 2002 *Appl. Phys. Lett.* **81** 2026
- [32] Cheng C and Zhao Y 2006 *Appl. Phys. Lett.* **89** 252501
- [33] Pan X F, Shen T M, Li G, Cheng C H and Zhao Y 2007 *Phys. Status Solidi a* **204** 1555
- [34] Ojha N, Malik V K, Bernhard C and Varma G D 2009 *Physica C* **469** 846
- [35] Ojha N, Malik V K, Bernhard C and Varma G D 2009 *Phys. Status Solidi a* **1** doi:10.1002/pssa.200925180
- [36] Ojha N, Varma G D, Singh H K and Awana V P S 2009 *J. Appl. Phys.* **105** 07E315
- [37] Paranthaman M, Thompson J R and Christen D K 2001 *Physica C* **355** 1
- [38] Takenobu T, Ito T, Chi D H, Prassides K and Iwasa Y 2001 *Phys. Rev. B* **64** 134513
- [39] Zhang X, Ma Y, Gao Z, Wang D, Yu Z and Wang L 2007 *Supercond. Sci. Technol.* **20** 1198
- [40] Beans C P 1964 *Rev. Mod. Phys.* **36** 31
- [41] Yeoh W K, Kim J H, Horvat J, Xu X, Qin M J, Dou S X, Jiang C H, Nakane T, Kumakura H and Munroe P 2006 *Supercond. Sci. Technol.* **19** 596
- [42] Williamson G K and Hall W H 1953 *Acta Metall.* **1** 22
- [43] Liao X Z, Serquis A, Zhu Y T, Peterson D E, Mueller F M and Xu H F 2004 *Supercond. Sci. Technol.* **17** 1026
- [44] Kim J H, Dou S X, Sangjun Oh, Jerčinović M, Babić E, Nakane T and Kumakura H 2008 *J. Appl. Phys.* **104** 063911
- [45] Kim J H, Oh S, Xu X, Joo J, Rindfleisch M, Tomsic M and Dou S X 2009 *J. Nanosci. Nanotechnol.* **9** 7477
- [46] Sequis A, Zhu Y T, Peterson E J, Coulter J Y, Peterson D E and Mueller F M 2001 *Appl. Phys. Lett.* **79** 4399
- [47] Rowell J M 2003 *Supercond. Sci. Technol.* **16** R17
- [48] Canfield C, Finnemore D K, Bud'ko S L, Ostenson J E, Lapertot G, Cunningham C E and Petrovic C 2001 *Phys. Rev. Lett.* **86** 2423
- [49] Zhang Y, Zhou S H, Lu C, Konstantinov K and Dou S X 2009 *Supercond. Sci. Technol.* **22** 015025
- [50] Matsumoto A, Kitaguchi H and Kumakura H 2008 *Supercond. Sci. Technol.* **21** 065007
- [51] Vinod K, Neson V, Roy S B and Syamaprasad U 2009 *Supercond. Sci. Technol.* **22** 055009
- [52] Vajpayee A, Awana V P S, Bhalla G L and Kishan H 2008 *Nanotechnology* **19** 125708
- [53] Zhang X, Wang D, Gao Z, Wang L, Ma Y, Qi Z and Watanabe K 2008 *Supercond. Sci. Technol.* **21** 075008
- [54] Dou S X, Braccini V, Soltanian S, Klie R, Zhu Y, Li S, Wang X L and Larbalestier D 2004 *J. Appl. Phys.* **96** 7549
- [55] Yamamoto A, Shimoyama J, Ueda S, Katsura Y, Iwayama I, Horii S and Kishio K 2005 *Appl. Phys. Lett.* **86** 212502
- [56] Serquis A, Serrano G, Moreno S M, Civalé L, Maiorov B, Balakirev F and Jaime M 2007 *Supercond. Sci. Technol.* **20** L12
- [57] Dew-Huges D 1987 *Phil. Mag. B* **55** 459
- [58] Tarantini C *et al* 2007 *Physica C* **463** 211
- [59] Cheng C H, Yang Y, Munroe P and Zhao Y 2007 *Supercond. Sci. Technol.* **20** 296